CYBERNETICS AND PHYSICS, VOL. 13, NO. 4, 2024, 334–345

NEURAL NETWORKS WITH ITERATIVE PARAMETER GENERATION FOR DETERMINING PARAMETERS OF CONSTITUTIVE MODELS

Yuyi Zhang
Faculty of Mathematics and Mechanics
St. Petersburg State University
Russia
lesliezhang0825@gmail.com

Shixiang Zhao
Faculty of Mathematics and Mechanics
St. Petersburg State University
Russia
zhaoshixiang@yandex.ru

Nikita Kazarinov
Faculty of Mathematics and Mechanics
St. Petersburg State University
Russia

Yuri V. Petrov
Institute for Problems in Mechanical Engineering
of the Russian Academy of Sciences
Russia

Article history:
Received 01.11.2024, Accepted 24.12.2024

Abstract

Determining the parameters of constitutive models is typically a material-specific process that requires recalibration when the material changes. This procedure becomes notably time-consuming with an increased number of parameters and integral terms in the constitutive equations. Recently, a novel approach utilizing neural networks has emerged as an alternative. By training neural networks to replace constitutive equations, constitutive substitution method maps the extensive parameter space to computational results equivalent to those derived from original equations. Comparing these results with experimental data allows for efficient determination of optimal parameter vectors. The powerful fitting capabilities and rapid computational speed of neural networks significantly expedite the parameter determination process. Consequently, the task of solving for parameters transitions from a complex optimization problem to a straightforward computational search. In this work, we introduce an iterative parameter generation (IPG) algorithm to enhance this substitution method, thereby improving its ability to fit a diverse range of materials. Additionally, we explore the benefits of constructing a general parameter space applicable to various material classes.

Key words

Constitutive model, Determination of parameters, Artificial neural network, Iterative generative algorithms

1 Introduction

Neural networks have received increasing attention in the field of mechanics in recent years, and a large number of studies have focused on their applications in the field (Le Viet et al., 2024; Gromov et al., 2024; Istomin and Pavlov, 2024; Andreevic, 2023). Constitutive modeling is crucial for analyzing mechanical properties, as it offers mathematical frameworks that predict material responses under different loads and environmental conditions (Savaedi et al., 2022; Ng et al., 2020). These models define the relationships between stress, strain, temperature, and other relevant variables (Zhao et al., 2024; Tricarico et al., 2023; Masri, 2023; Haikova et al., 2020; Alkhatib and Sercombe, 2022). This capability enables engineers and scientists to predict material behavior, optimize designs, conduct failure analyzes, and make informed decisions on material selection. In recent years, the use of neural networks to explore the constitutive relations of materials has attracted significant attention. This interest is largely driven by the universal approximation theorem, which posits that neural networks can theoretically approximate any function (Liu et al., 2021; Dornheim et al., 2024; Holthusen et al., 2024). However, this powerful fit ability comes with a significant drawback: overfitting remains a fundamental issue in machine learning and deep learning, garnering substantial focus within the field of artificial intelligence (Kou et al., 2023; Xu and Gu, 2023; Kornowski et al., 2024). Furthermore, another critical limitation is the lack of a rigorous framework of physical laws within the neural network paradigm. This absence often leads to inconsis-

tencies from a physical point of view (Masi et al., 2021; Xu et al., 2021; Chen and Guilleminot, 2022; Su et al., 2024; Idrissi et al., 2024). These issues pose substantial risks for practical engineering applications, where such inconsistencies can have severe consequences.

To address the challenges associated with using neural networks in constitutive modeling, extensive research has focused on integrating physical principles into these networks (Chiu et al., 2022; Yuan et al., 2022; Bararnia and Esmaeilpour, 2022; Meng et al., 2023; Zhang et al., 2022). A prominent approach involves embedding thermodynamic principles. For instance, (Masi et al., 2021) developed a Thermodynamics-based Artificial Neural Network (TANN) by incorporating thermodynamic knowledge into a neural network. This method proved effective for modeling various elastic-plastic materials, including those exhibiting hyper-plasticity and hypo-plasticity. Building on this approach, (Su et al., 2024) introduced the Thermodynamics-Informed Neural Network (TINN), which replaces the traditional neural network with a recurrent neural network (RNN). This substitution allows TINN to account for temporal relationships inherent in the constitutive models, thus providing more generalized and stable modeling capabilities. (Idrissi et al., 2024) concentrated on inelastic composites, which typically demand significant computational resources. They leveraged the relatively efficient computation of ANN by embedding multi-scale thermodynamic information, thereby enhancing the modeling of composite structures. Furthermore, advancements at the mathematical level have also contributed to the improved modeling of material properties. (Xu et al., 2021) incorporated the Cholesky factor into the neural network to develop a symmetric positive definite neural network (SPD-NN). This innovation introduces weak convexity to the strain energy function, thereby stabilizing numerical computations. Similarly, (Chen and Guilleminot, 2022) proposed a corrective method that enhances both the stability and consistency of neural networks by integrally representing forced convexity. These efforts underscore the potential of embedding physical and mathematical principles into neural networks to improve their performance in constitutive modeling, leading to more accurate and reliable predictions.

However, despite these advancements, neural networks remain inherently non-interpretable (Dwivedi et al., 2023; Saeed and Omlin, 2023; Arrieta et al., 2020; Minh et al., 2022; de Bruijn et al., 2022). Their "black-box" nature allows them to produce highly accurate fitting results but does not enable researchers to further analyze or compute the mechanical properties of materials, as traditional constitutive equations do. Consequently, leveraging neural networks to determine parameters for established constitutive models represents a promising research direction with significant potential for practical applications (Wang et al., 2021, 2023; Veasna et al., 2023; Pogorelko et al., 2024). The present work builds upon the methodologies established by (Wang et al., 2021) and (Wang et al., 2023), which utilize neural networks to replace constitutive models—referred to as substitution methods. These methods transform the problem of parameter determination from a complex optimization task into a straightforward computer lookup operation within a large parameter space. (Pogorelko et al., 2024) constructed both forward and inverse problems using neural networks, allowing for direct output of parameters from the inverse problem network. In contrast, (Veasna et al., 2023) employs a Pareto-based multi-objective machine learning technique to identify the parameters. This study continues along the lines set by (Wang et al., 2021) and (Wang et al., 2023), leveraging their innovative approaches to solving parameter determination. This paradigm shift represents a significant advancement over traditional optimization algorithms. For instance, consider the constitutive model G_{pva} for PVA (Polyvinyl alcohol) material in work of (Wang et al., 2021):

$$\sigma(\vec{\theta},t)=\left[\mu\rho+\mu\bar{\gamma}\frac{t_B}{2-\alpha_B}(1+(\alpha_B-1)\frac{t}{t_B}^{\frac{2-\alpha_B}{1-\alpha_B}})\right]\times\left[\lambda(t)-\frac{1}{\lambda^2(t)}\right]+\mu\bar{\gamma}\int_0^t\phi_B(\frac{t-\tau}{t_B})\left[\frac{\lambda(t)}{\lambda^2(\tau)}-\frac{\lambda(\tau)}{\lambda^2(t)}\right]d\tau \tag{1}$$

where $\phi_B(\frac{t}{t_B})=(1+(\alpha_B-1)\times\frac{t}{t_B})^{\frac{1}{1-\alpha_B}}$, $\lambda(t)$ is the stretch ratio and $\vec{\theta}=(\mu\rho,\alpha_B,t_B,\mu\bar{\gamma})$ is the parameter vector with $n=4$ parameters of the constitutive model that needs to be determined.

When 10^6 parameter vectors $\vec{\theta}$ are randomly generated and used to compute the stress response histories $\sigma(\vec{\theta},t)$ through the constitutive model (Equ.(1)), we can directly identify the vector that best matches the experimental data. This allows us to output the corresponding parameter values immediately. Essentially, this method transforms the parameter determination from an optimization problem into a straightforward lookup problem for the computer. However, the primary challenge with this approach lies in the computational demands of the constitutive model. Performing 10^6 computations with the constitutive model can be prohibitively time-consuming. For instance, as reported by (Wang et al., 2023), these computations took a total of 4.6 hours. The core innovation of the substitution method involves using neural networks in place of the constitutive model, facilitating efficient computation on large datasets. In comparison, the same 10^6 computations with a neural network model, as documented by (Wang et al., 2023), required merely 0.34 seconds, with the model training taking 72 seconds. This progression from traditional constitutive models to neural networks represents a significant advancement, offering substantial improvements in computational ef-

ficiency.

Theoretically, the 10^6 parameter vectors mentioned correspond to 10^6 different materials. This suggests that the substitution method could identify parameters for a class of materials that conform to the same constitutive equations, not just a single material. We believe this is where the substitution method holds significant potential for development. However, there are still several problems remained. Beyond the unexplored potential, the substitution method faces a crucial challenge: can neural networks accurately replace the original constitutive model? Specifically, can the neural network's output maintain consistency or approximate the stress response history using the same parameter vectors as those in the constitutive equations? The key to addressing this issue lies in setting appropriate ranges for the parameters. A smaller range results in more accurate neural network substitutions. In the work (Wang et al., 2023), parameter ranges were explicitly set based on experience, and the values themselves were relatively small for PVA material constitutive equations. However, when applied to new materials or materials with larger parameter values, the neural network often fails to accurately substitute the constitutive model, leading to the method's failure. To address the challenge of determining appropriate parameter value ranges and to further explore the potential of substitution methods, we have outlined a technical approach for the constitutive substitution method. Our work offers the following key contributions:

1. Iterative Parameter Generation (IPG) Algorithms: We developed algorithms that iteratively generate parameters, thereby expanding the range of possible values. This enhancement increases the applicability of the constitutive substitution method across various scenarios.
2. Simultaneous Parameter Identification for Multiple Materials: We leveraged the method's capability to concurrently determine parameters for two different metallic materials using the same constitutive equation. This dual identification process highlights the method's efficiency and broadens its practical utility.

The Section 2 provides a detailed description of the problem and introduces the associated symbols used in our expressions. In the Section 3, we discuss the constitutive substitution method, including the iterative generation of parametric algorithms and the technical approach employed. The experimental results and discussion are presented in Section 4. Finally, Section 5 concludes the paper, summarizing the key findings and implications of our work.

2 Statement of problems

For the constitutive models, in the constitutive substitution method, the parameter space Θ is mapped to the stress response space Ω: $\Theta \to \Omega$ by a neural network f, where $\Theta = \left\{\vec{\theta}_1, \vec{\theta}_2, \cdots, \vec{\theta}_p\right\}$, $\Theta \subset \mathbb{R}^n$, n is the number of parameters, and

$$\Omega = \left\{\sigma_1(\vec{\theta}_1, \vec{t}), \sigma_2(\vec{\theta}_2, \vec{t}), \cdots, \sigma_p(\vec{\theta}_p, \vec{t})\right\}, \Omega \subset \mathbb{R}^m,$$

$$\sigma_i(\vec{\theta}_i, \vec{t}) = \left\{\sigma_i(\vec{\theta}_i, t_1), \sigma_i(\vec{\theta}, t_2), \cdots \sigma_i(\vec{\theta}_i, t_m)\right\},$$
$$\vec{t} = (t_1, \cdots, t_m).$$

The data used to train the neural network model is obtained through the constitutive model G_{pva}, i.e.

$$\sigma_i(\vec{\theta}_i, \vec{t}) = G_{pva}(\vec{\theta}_i, \vec{\lambda}(t), \vec{t}),$$
$$\vec{\lambda}(t) = \left\{\vec{\lambda}(t_1), \cdots, \vec{\lambda}(t_m)\right\},$$

Firstly, 1000 parameter vectors are randomly generated, i.e. p =1000, and correspondingly 3000 training data will be computed accordingly. Use this data to train the neural network model f:

$$f(\vec{\theta}_i) = \sigma_i(\vec{\theta}_i, \vec{t})$$

The main goal of the substitution method is to achieve $f(\Theta) \approx G_{pva}(\Theta, \vec{\lambda}(t), \vec{t})$.

Based on our previous discussion of this substitution method, it is evident that the neural network's ability to accurately substitute constitutive equations hinges on its capacity to produce outputs consistent with those models given identical inputs. Our research indicates that a critical factor in achieving this accuracy is the range of parameters used to generate random values, predetermined by us. Narrowing this parameter range enhances the quality of the neural network's approximation of the constitutive equations. To illustrate the impact of parameter range settings on substitution quality, we present an example using the original paper's constitutive model Equ.(1). The options for the value ranges of the parameters are shown in Table 1. In particular, option 1 is derived from the empirical values set in the original paper, on the basis of which we gradually narrowed down the range of values of the parameters to constitute the other options.

Table 1. Options for parameter value ranges

options	$\mu\rho$	α_B	t_B	$\mu\bar{\gamma}$
1	[0, 15]	[1.3, 1.9]	[0, 1.5]	[0, 100]
2	[0, 10]	[1.4, 1.8]	[0.1, 1.0]	[20, 80]
3	[2, 8]	[1.4, 1.7]	[0.1, 0.5]	[40, 70]
4	[2, 6]	[1.5, 1.7]	[0.2, 0.4]	[50, 70]
5	[3, 6]	[1.6, 1.7]	[0.2, 0.3]	[60, 70]

After configuring the options, we begin by randomly generating 1000 sets of parameters and obtaining the corresponding stress response data. This data is used to train the neural network. Next, we regenerate the 1000 sets of parameters along with their stress response data to assess the neural network's accuracy in fitting the constitutive equations. The error is calculated using the following formula:

$$e_{val} = \frac{1}{|\Omega|} \sum \frac{\|\vec{\sigma}_i - \vec{\sigma}_i^c\|}{\|\vec{\sigma}_i^c\|} \tag{2}$$

where $\vec{\sigma}_i$ is the output from the neural network and $\vec{\sigma}_i^c$ is the output from the constitutive models.

Figure 1 illustrates how the neural network's capacity to substitute constitutive equations improves with different parameter range options. A smaller error signifies a higher quality of substitution. Clearly, as the range of values becomes more restricted, the neural network's substitution ability progressively enhances.

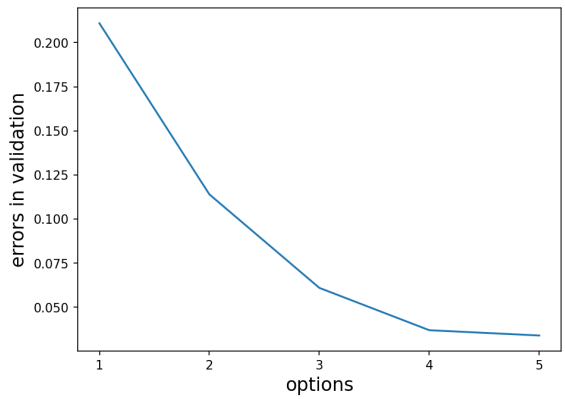

Figure 1. Effect of parameter value ranges on validation error, and parameter value range options in Table 1.

Through addressing these limitations, we aim to further refine and validate the substitution method as a robust tool for determining parameters of constitutive models.

3 Methods and techniques

3.1 Thermal softening of metals and the constitutive model

Thermal softening (Goviazin et al., 2023; Zhang et al., 2021a; Hao et al., 2022; Shen et al., 2020) is the reduction in a metal's strength and hardness as the temperature increases. This phenomenon significantly affects mechanical properties such as yield strength, tensile strength, and ductility. As the temperature rises, atomic vibrations become more intense, weakening the metallic bonds and facilitating dislocation movement within the crystal structure (Li et al., 2020; Gao et al., 2022; Safina et al., 2022; Zhu et al., 2024; Li et al., 2024). Consequently, the metal deforms more easily under stress. Elevated temperatures also enhance dislocation mobility, which can lead to recrystallization (Zhang et al., 2020; Tiamiyu et al., 2022; Derazkola et al., 2022; Zhang et al., 2021b; Li et al., 2021). During recrystallization, new grains with fewer dislocations form, reducing strength but increasing ductility. Moreover, high temperatures can cause phase transformations in certain alloys, altering their crystalline structure and further impacting their hardness and strength.

The strain-stress relationship of a material outlines how it deforms under an applied load, and thermal softening significantly influences this interaction. As temperature increases, the yield strength (Giles et al., 2022; Liu et al., 2020; Hou et al., 2022; Deng et al., 2020) -the stress at which a material begins to plastically deform- decreases. This reduction means that the material yields at lower stresses when exposed to high temperatures compared to cold conditions. Similarly, the ultimate tensile strength, which represents the maximum stress a material can endure before breaking, diminishes as temperature rises. Consequently, materials become less capable of withstanding high loads without failing at elevated temperatures. Increased ductility, or the ability of a material to undergo substantial plastic deformation before rupture, is another effect of higher temperatures. Metals exhibit greater elongation and reduction in area before fracturing when tested at elevated temperatures. Additionally, the rate at which a metal strengthens due to plastic deformation, known as the work hardening rate, tends to decrease with rising temperature. This results in a less steep slope in the strain-hardening portion of the stress-strain curve. As a result, the typical stress-strain curve shifts noticeably with temperature variations. At low temperatures, materials display high yield strength, high ultimate tensile strength, and low ductility. Conversely, at high temperatures, materials exhibit lower yield strength, lower ultimate tensile strength, and increased ductility.

Zerilli-Armstrong (ZA) models (Zerilli and Armstrong, 1987, 1996) are a version of dislocation-mechanics-based (Dm) models. The motion of dislocations plays a pivotal role in influencing plastic deformation. The presence of defects within a material that contains dislocations can impede the motion of these dislocations, leading to interactions between them. To overcome this impediment, a flow stress σ, must be generated. This flow stress can be decomposed into two distinct components, as expressed in Equation 3. The general form of the model can be written as:

$$\sigma = \sigma_{ath} + \sigma_{th} \tag{3}$$

where the thermal component, denoted as σ_{th}, can be derived through various relationships within the framework of dislocation kinetics. The form of the athermal component, represented as σ_{ath}, may be informed and guided by empirical experimental results.

The ZA model G_{za} encompasses body-centered cubic (BCC), face-centered cubic (FCC), and hexagonal close-packed (HCP) crystal structures. Building on previous research, the constitutive model for BCC metals can be expressed as follows:

$$\sigma(\vec{\theta}) = \sigma_{ath} + B \times e^{-\beta_0 T + \beta_1 T \ln\dot{\varepsilon}} + B_0 \varepsilon_p^n \quad (4)$$

where the parameter vector $\vec{\theta} = (\sigma_{ath}, B, \beta_0, \beta_1, B_0, n)$, correspondingly, $\Theta \subset \mathbb{R}^n$, $n = 6$.

The first term σ_{ath} accounts for the athermal component. This component is independent of temperature T and remains constant under various conditions. The second term results from the thermal activation analysis of Peierls stress interactions. This term captures the temperature-dependent behavior of the material, illustrating how thermal energy affects the movement of dislocations. It is important to note that $\dot{\varepsilon}$ represents the strain rate in this context. The third term represents continuous work hardening, where the material's resistance to deformation increases without reaching a maximum flow stress at large strains. In scenarios involving isotropic hardening, this hardening parameter is typically associated with the equivalent plastic strain ε_p.

During plastic deformation, the process of temperature rise occurs as heat is produced within the material. This heat can either escape to the surrounding environment or be retained internally, thereby increasing the material's temperature. When the rate at which heat is generated exceeds the rate at which it is dissipated, the material's temperature begins to rise. In scenarios involving high strain rates, an adiabatic process may occur. Here, the rapid and intense nature of plastic deformation results in most of the generated heat being trapped within the material, leading to a significant increase in temperature. As this happens, there is a concurrent decrease in the material's flow stress, impacting its deformation behavior. The quantitative assessment of this temperature increase is typically governed by a specific equation, referenced as Eq. (5) for the one-dimensional case.

$$\Delta T = \frac{\eta}{\rho C_v} \int \sigma d\varepsilon_p \quad (5)$$

where ρ is the mass density, η is the plastic work-heat conversion factor, and C_v is heat capacity.

3.2 Structure of the artificial neural network

In the original study, an adaptive neural network framework was utilized. This framework allowed for the number of layers in the network to be dynamically increased based on feedback from a validation set, enhancing the accuracy of the neural network as a substitute for the constitutive model. However, our research suggests that the range of parameters has a more significant impact than the structure of the neural network itself. We find that when the parameter range is constrained within a narrow band, a simpler neural network with just two hidden layers can effectively replace the constitutive model.

The fundamental structure of a classical neural network comprises three main components: the input layer, the hidden layers, and the output layer (Zou et al., 2009; Yegnanarayana, 2009; Basheer and Hajmeer, 2000). Each layer contains a pre-determined number of neurons. In our study, the input layer consists of 6 neurons (number of parameters). The hidden layers include two layers, each with 32 neurons. The number of neurons in the output layer corresponds to the number of stress histories m, which varies according to the experimental conditions. In the first hidden layer of our neural network, each neuron executes a computation represented by $\mathbf{w}_{1k}\vec{\theta}+b_{1k}$, where $\vec{\theta}$ is the input vector from the input layer, $\mathbf{w}_{1k}$ denotes the weight vector, and b_{1k} is the bias term. Similarly, the neurons in the second hidden layer follow the same operational form using their respective weights $\mathbf{w}_{2k}$ and biases b_{2k}. Finally, the output layer processes its inputs with the corresponding weights $\mathbf{w}_{3k}$ and biases b_{3k}, producing the final output of the neural network.

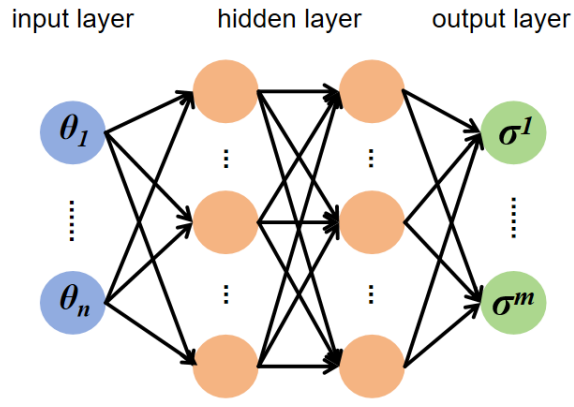

Figure 2. Bi-layer neural network structure. The neural network utilized in this study has a bi-layer structure. The input layer comprises six neurons, corresponding to the six parameters of the constitutive model (represented by blue circles). The hidden consists of two layers, each containing 32 neurons (depicted as orange circles). Finally, the output layer produces a specific stress history, illustrated by green circles.

This operation's result is then processed through an activation function a, and passed to the next layer, where a same computation occurs. The activation function a is:

$$a(z) = \ln(1 + e^z) \quad (6)$$

Correspondingly, the first hidden layer follows this structure and can be denoted as follows:

$$h_{1k}(\vec{\theta}) = \ln(1 + e^{\mathbf{w}_{1k}\vec{\theta}+b_{1k}}) \quad (7)$$

And the second hidden layer follows:

$$h_{2k}(h_1) = \ln(1 + e^{\mathbf{w}_{2k}h_1 + b_{2k}}) \quad (8)$$

Finally, at the output layer, the output is given by:

$$f(\vec{\theta}) = \mathbf{w}_{3i} \times h_2 + b_{3i}, \quad i = 1, 2, \cdots, m \quad (9)$$

By continually narrowing down the range of parameters so as to eventually achieve $f(\Theta) \approx G_{za}(\Theta, \dot{\varepsilon}, \varepsilon_p)$.

3.3 Iterative parameter generation algorithm

For metal materials, the parameter values can be quite large, resulting in an expanded range of potential values. This makes the previously mentioned strategy of randomly generating parameter vectors impractical for neural networks to effectively substitute the constitutive equations. To address this challenge and improve the applicability of the substitution method for materials with a wide range of parameter values, we have developed an iterative parameter generation algorithm (Fig.3). The process begins by randomly generating 3,000 initial parameter vectors, which are used to calculate corresponding stress histories. These stress histories serve as training data for a neural network model, enabling it to predict stress responses based on these parameters.

Next, a much larger set of 3 million parameter vectors is generated to create a comprehensive stress response history matrix. This matrix, consisting of prediction data, is then refined using experimental stress data. Initially, for example, experimental data at $T = 500, \dot{\varepsilon} = 8500$ is compared with the matrix. By filtering out entries with errors less than 5, the algorithm forms a refined matrix, effectively narrowing the parameter space. The refinement continues with another set of experimental data at $T = 700, \dot{\varepsilon} = 8500$. Again, only predictions with minimal errors are retained, further tightening the parameter range. This filtered dataset is then used to define a new, narrower range of parameter vectors, which leads back to the initial step of the algorithm. By iteratively applying this process, the algorithm systematically reduces the range of parameter values, thereby improving the precision and reliability of the neural network's stress response predictions. This targeted refinement ensures that the parameter space becomes increasingly defined, leading to more accurate and dependable predictions.

4 Results and discussion

In this study, we evaluate the effectiveness of the constitutive substitution method on metal materials, specifically steel and iron. This approach differs from traditional parameter-solving techniques as it employs IPG algorithm to simultaneously determine the parameters for both types of metals.

4.1 HSLA-65 Steel

Compression tests were conducted over a broad spectrum of strain rates, ranging from 0.001/s to 8500/s, and temperatures from 77 K to 1000 K. For quasi-static loading rates of 0.001/s and 0.1/s, an Instron hydraulic testing machine was utilized, with tests performed at temperatures from 77 K to 800 K (Nemat-Nasser and Guo, 2005). Elevated temperatures were achieved with a high-intensity quartz lamp within a radiant-heating furnace in an argon environment. Conversely, the low temperature of 77 K was attained by immersing both the specimen and the testing fixture in liquid nitrogen. High strain rate tests were executed using the enhanced compression recovery Hopkinson technique, covering a temperature range from 77 K to 1000 K. At temperatures above 700 K, an unusual increase in flow stress was observed due to dynamic strain aging. This phenomenon is beyond the scope of the current paper; hence, our modeling focuses on the temperature range of 77 K to 700 K. For HSLA-65 Steel, in Eq. (5), $\rho = 7.8g/cc$, $\eta = 1$, $C_v = 0.5J/gk$.

After giving a range of values to the parameter vector, the iterative generative algorithm can be used to reduce this range, and the results of each iteration are displayed in the Table 2. The experiment results demonstrate that with an increase in iterations, the parameter values become more precise. This refinement enables the constitutive substitution method to identify parameters within a limited range effectively. Table 3 presents the parameters determined by both the constitutive substitution method and the optimization algorithm, highlighting their average errors for steel materials. The the visualisation of the simulation results is presented in Figure 4.

4.2 93W-4.9Ni-2.1Fe Tungsten-based composite

(Xu and Huang, 2013) investigated the mechanical behavior of a commercial tungsten-based composite (93W-4.9Ni-2.1Fe) with a body-centered cubic (BCC) structure. They conducted tests across a broad spectrum of strain rates, from 0.001/s to 3000/s, and temperatures ranging from 288 K to 873 K. Dynamic compression tests at high strain rates of 1000/s and 3000/s were performed using a modified split Hopkinson pressure bar technique. These tests utilized electro-thermal cells to achieve elevated temperatures between 288 K and 873 K. For the quasi-static conditions, involving strain rates of 0.001/s, an MTS servo-hydraulic testing machine was employed. For 93W-4.9Ni-2.1Fe Tungsten-based composite, in Eq. (5), $\rho = 17.8g/cc$, $\eta = 0.9$, $C_v = 162.92 - 0.00995T + 1.74 \times 10^{-5}T^2 (\times 10^{-3} J/gK$, for $0°C \leq T \leq 1000°C$ (Xu and Huang, 2013).

After giving a range of values to the parameter vector, the iterative generative algorithm can be used to reduce this range, and the results of each iteration are displayed in the Table 4. The experiment results demonstrate that with an increase in iterations, the parameter values become more precise. This refinement enables the constitutive substitution method to identify parameters within a limited range effectively. Table 5 presents

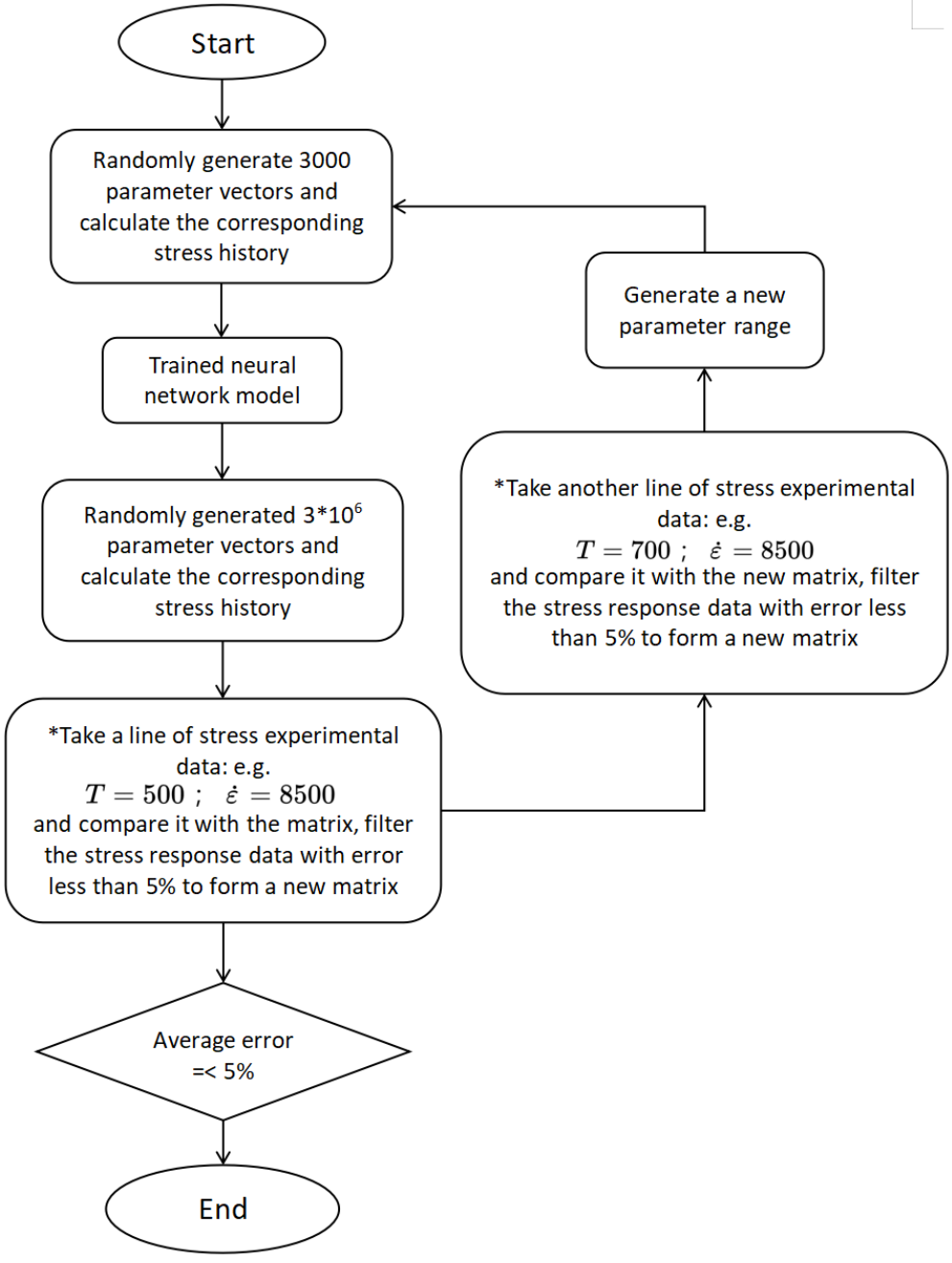

Figure 3. Flowchart of the iterative parameter generation (IPG) algorithm

the parameters determined by both the IPG method and the optimization algorithm - least square (LS) method, highlighting their average errors for steel materials. The the visualisation of the simulation results is presented in Figure 5.

5 Conclusion

In this paper, we introduce a groundbreaking neural network-based approach for determining the parameters of constitutive models, which we refer to as the constitutive substitution method. This innovative method is enhanced by integrating an iterative generation algorithm, significantly increasing the efficiency and accuracy of exploring the parameter space for precise parameter determination. The iterative nature of our algorithm allows for continuous refinement and optimization, reducing computational resources while enhancing reliability.

Moreover, we extend the applicability of this method across various materials, enabling simultaneous parameter determination for different substances governed by the same constitutive equations. This cross-material capability not only streamlines the modeling process but also facilitates a broader understanding of material behaviors under similar theoretical frameworks. By im-

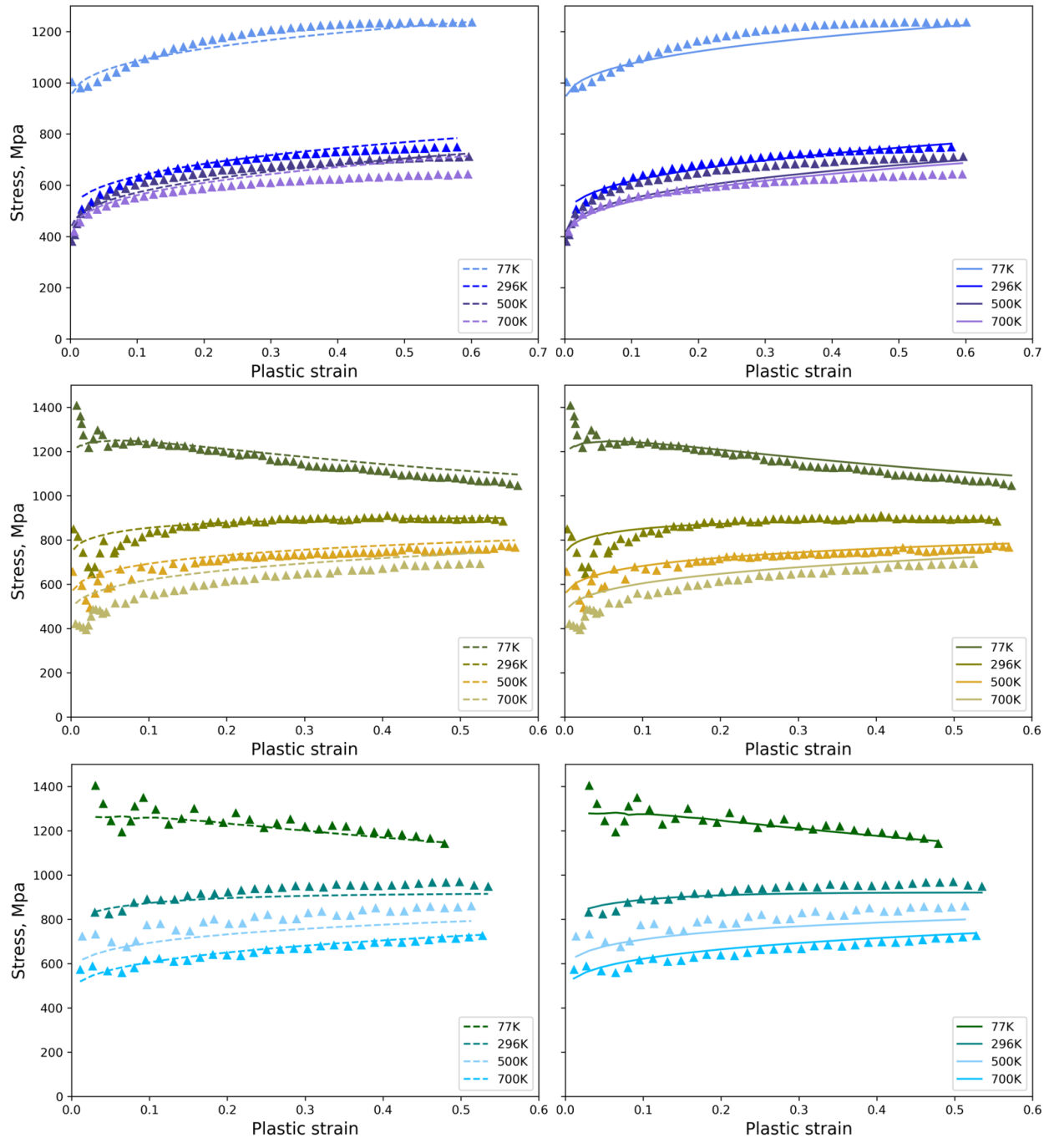

Figure 4. Stress-strain diagrams of HSLA-65 steel at 4 temperatures and 2 high loading rates and corresponding simulation results. The dashed line on the left shows the simulation results of the IPG -(a), (c), (e), while the solid line on the right shows the simulation results of the least square -(b), (d), (f) (Zhao et al., 2024) .

proving both the efficiency of parameter exploration and the versatility of application, our method offers a robust and comprehensive tool for researchers and engineers in the field of constitutive modeling.

Acknowledgements

We hereby acknowledge the financial support from the RSF, which was instrumental in facilitating the research efforts of Yuyi Zhang and Nikita Kazarinov under grant 22-71-10019.

References

Alkhatib, S. E. and Sercombe, T. B. (2022). High strain-rate response of additively manufactured light metal alloys. *Materials & Design*, **217**, pp. 110664.

Andreevic, K. N. (2023). Forecasting the state of complex network systems using machine learning meth-

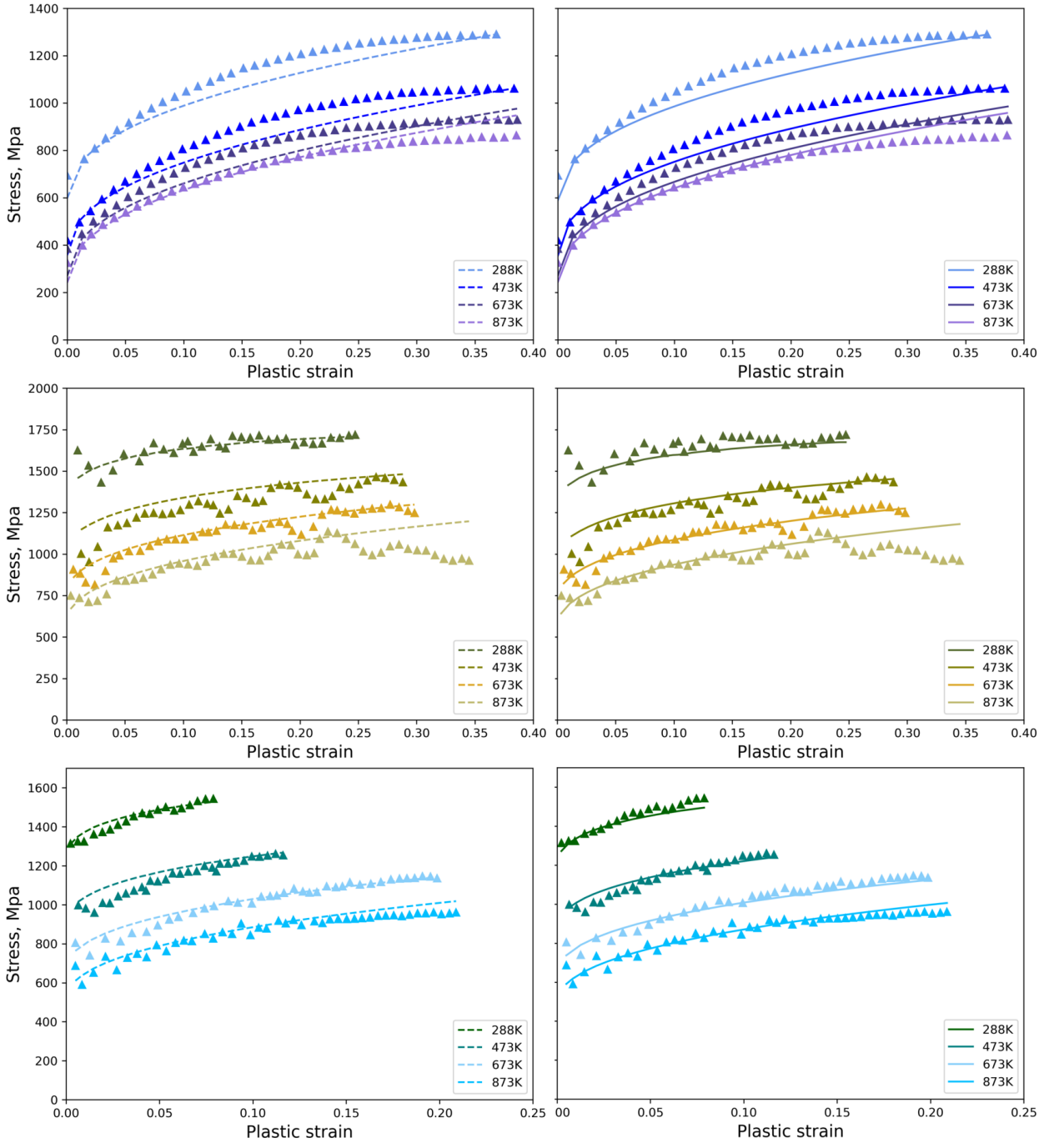

Figure 5. Stress-strain diagrams of 93W-4.9Ni-2.1Fe Tungsten-based composite at 4 temperatures and 2 high loading rates and corresponding simulation results. The dashed line on the left shows the simulation results of the IPG -(a), (c), (e), while the solid line on the right shows the simulation results of the least square -(b), (d), (f) (Zhao et al., 2024).

ods. *CYBERNETICS AND PHYSICS*, **12** (2), pp. 129–135.

Arrieta, A. B., Díaz-Rodríguez, N., Del Ser, J., Bennetot, A., Tabik, S., Barbado, A., García, S., Gil-López, S., Molina, D., Benjamins, R., et al. (2020). Explainable artificial intelligence (xai): Concepts, taxonomies, opportunities and challenges toward responsible ai. *Information fusion*, **58**, pp. 82–115.

Bararnia, H. and Esmaeilpour, M. (2022). On the application of physics informed neural networks (pinn) to solve boundary layer thermal-fluid problems. *International Communications in Heat and Mass Transfer*, **132**, pp. 105890.

Basheer, I. A. and Hajmeer, M. (2000). Artificial neural networks: fundamentals, computing, design, and application. *Journal of microbiological methods*, **43** (1), pp. 3–31.

Chen, P. and Guilleminot, J. (2022). Polyconvex neu-

Table 2. Iterations for parameter value ranges for HSLA-65 Steel

Iterations	σ_{ath}(MPa)	B(MPa)	$\beta_0(K^{-1})$	$\beta_1(K^{-1})$	B_0(MPa)	n
1	[200.0, 400.0]	[1000.0, 2000.0]	[3.0e-3, 7.0e-3]	[2.0e-4, 4.0e-4]	[300.0, 1200.0]	[0.30, 0.50]
2	[200.0, 399.9]	[1000.0, 1999.9]	[3.4e-3, 6.9e-3]	[2.0e-4, 3.9e-4]	[300.0, 757.73]	[0.30, 0.49]
3	[347.2, 399.5]	[1004.0, 1264.7]	[6.5e-3, 6.9e-3]	[2.0e-4, 3.8e-4]	[300.9, 506.76]	[0.30, 0.36]
4	[347.2, 399.4]	[1004.0, 1264.7]	[6.5e-3, 6.8e-3]	[2.1e-4, 3.7e-4]	[308.5, 506.75]	[0.30, 0.35]
5	[347.2, 394.9]	[1004.0, 1264.6]	[6.5e-3, 6.8e-3]	[2.1e-4, 3.4e-4]	[323.0, 413.05]	[0.30, 0.35]
6	[347.2, 388.8]	[1004.0, 1264.6]	[6.5e-3, 6.8e-3]	[2.3e-4, 3.4e-4]	[329.9, 404.59]	[0.30, 0.35]
7	[347.2, 385.6]	[1004.0, 1259.0]	[6.5e-3, 6.8e-3]	[2.4e-4, 3.2e-4]	[331.0, 398.57]	[0.30, 0.35]

Table 3. Parameters values of HSLA-65 Steel determined by iterative parameter generation algorithm and least square method (LS).

Methods	σ_{ath}(MPa)	B(MPa)	$\beta_0(K^{-1})$	$\beta_1(K^{-1})$	B_0(MPa)	n	error
IPG	383.97	1037.08	6.58e-3	3.24e-4	392.67	0.35	4.08%
LS (Zhao et al., 2024)	361.74	1049.81	6.39e-3	3.23e-4	386.12	0.35	**3.81**%

Table 4. Iterations for parameter value ranges for 93W-4.9Ni-2.1Fe Tungsten-based composite

iterations	σ_{ath}(MPa)	B(MPa)	$\beta_0(K^{-1})$	$\beta_1(K^{-1})$	B_0(MPa)	n
1	[200.0, 400.0]	[1000.0, 2000.0]	[3.0e-3, 7.0e-3]	[2.0e-4, 4.0e-4]	[300.0, 1200.0]	[0.30, 0.50]
2	[200.0, 399.9]	[1305.1, 2000.0]	[3.2e-3, 6.7e-3]	[2.0e-4, 3.9e-4]	[621.3, 1200.0]	[0.31, 0.50]
3	[205.3, 366.2]	[1324.6, 1998.7]	[3.2e-3, 5.8e-3]	[2.2e-4, 3.9e-4]	[621.3, 1200.0]	[0.31, 0.48]
4	[205.3, 298.2]	[1556.7, 1998.7]	[3.5e-3, 5.8e-3]	[2.2e-4, 3.7e-4]	[700.6, 1163.8]	[0.35, 0.48]
5	[205.2, 288.9]	[1678.7, 1998.4]	[3.5e-3, 4.6e-3]	[2.2e-4, 3.5e-4]	[700.5, 1163.7]	[0.35, 0.45]
6	[212.6, 288.9]	[1678.1, 1998.4]	[3.7e-3, 4.6e-3]	[2.4e-4, 3.5e-4]	[996.6, 1102.1]	[0.35, 0.45]
7	[212.6, 288.8]	[1678.1, 1998.3]	[3.7e-3, 4.5e-3]	[2.4e-4, 3.5e-4]	[996.7, 1102.0]	[0.38, 0.45]

Table 5. Parameters values of 93W-4.9Ni-2.1Fe Tungsten-based composite determined by iterative parameter generation algorithm and least square method (LS).

Methods	σ_{ath}(MPa)	B(MPa)	$\beta_0(K^{-1})$	$\beta_1(K^{-1})$	B_0(MPa)	n	error
IPG	228.62	1902.35	3.95e-3	2.52e-4	1072.23	0.4383	3.98%
LS (Zhao et al., 2024)	230.50	1864.60	4.01e-3	2.49e-4	1083.10	0.4355	**3.70**%

ral networks for hyperelastic constitutive models: A rectification approach. *Mechanics Research Communications*, **125**, pp. 103993.

Chiu, P.-H., Wong, J. C., Ooi, C., Dao, M. H., and Ong, Y.-S. (2022). Can-pinn: A fast physics-informed neural network based on coupled-automatic–numerical differentiation method. *Computer Methods in Applied Mechanics and Engineering*, **395**, pp. 114909.

de Bruijn, H., Warnier, M., and Janssen, M. (2022). The perils and pitfalls of explainable ai: Strategies for explaining algorithmic decision-making. *Government information quarterly*, **39** (2), pp. 101666.

Deng, W., Zhang, D., Wu, H., Huang, Z., Zhou, K., and Jiang, L. (2020). Prediction of yield strength in a polycrystalline nickel base superalloy during interrupt cooling. *Scripta Materialia*, **183**, pp. 139–143.

Derazkola, H. A., Garcia, E., Murillo-Marrodán, A., and Fernandez, A. C. (2022). Review on modeling and simulation of dynamic recrystallization of martensitic stainless steels during bulk hot deformation. *Journal of Materials Research and Technology*, **18**, pp. 2993–3025.

Dornheim, J., Morand, L., Nallani, H. J., and Helm, D. (2024). Neural networks for constitutive modeling: From universal function approximators to advanced models and the integration of physics. *Archives of Computational Methods in Engineering*, **31** (2), pp. 1097–1127.

Dwivedi, R., Dave, D., Naik, H., Singhal, S., Omer, R., Patel, P., Qian, B., Wen, Z., Shah, T., Morgan, G., et al. (2023). Explainable ai (xai): Core ideas, techniques, and solutions. *ACM Computing Surveys*, **55** (9), pp. 1–33.

Gao, P., Yan, X., Li, F., Zhan, M., Ma, F., and Fu, M. (2022). Deformation mode and wall thickness variation in conventional spinning of metal sheets. *International Journal of Machine Tools and Manufacture*, **173**, pp. 103846.

Giles, S. A., Sengupta, D., Broderick, S. R., and Rajan, K. (2022). Machine-learning-based intelligent framework for discovering refractory high-entropy alloys with improved high-temperature yield strength. *npj Computational Materials*, **8** (1), pp. 235.

Goviazin, G. G., Shirizly, A., and Rittel, D. (2023). Does plastic anisotropy affect the thermo-mechanical coupling in steel? *International Journal of Engineering Science*, **187**, pp. 103852.

Gromov, N. V., Smirnov, L. A., and Levanova, T. A. (2024). Prediction of extreme events and chaotic dynamics using wavenet. *CYBERNETICS AND PHYSICS*, **13** (1), pp. 20–31.

Haikova, T., Puzyr, R., and Levchenko, R. (2020). Experimental studies on the stress-strain state under drawing aluminum–copper bimetal parts rectangular in plan. *Russian Journal of Non-Ferrous Metals*, **61**, pp. 404–412.

Hao, P., Laheri, V., Dai, Z., and Gilabert, F. (2022). A rate-dependent constitutive model predicting the double yield phenomenon, self-heating and thermal softening in semi-crystalline polymers. *International Journal of Plasticity*, **153**, pp. 103233.

Holthusen, H., Lamm, L., Brepols, T., Reese, S., and Kuhl, E. (2024). Theory and implementation of inelastic constitutive artificial neural networks. *Computer Methods in Applied Mechanics and Engineering*, **428**, pp. 117063.

Hou, K., Wang, M., Zhao, P., Ou, M., Li, H., Ma, Y., and Liu, K. (2022). Temperature-dependent yield strength and deformation mechanism of a casting ni-based superalloy containing low volume-fraction γ phase. *Journal of Alloys and Compounds*, **905**, pp. 164187.

Idrissi, M. E. F., Praud, F., Meraghni, F., Chinesta, F., and Chatzigeorgiou, G. (2024). Multiscale thermodynamics-informed neural networks (mutinn) towards fast and frugal inelastic computation of woven composite structures. *Journal of the Mechanics and Physics of Solids*, **186**, pp. 105604.

Istomin, V. A. and Pavlov, S. A. (2024). Suitability of different machine learning methods for high-speed flow modelling issues. *CYBERNETICS AND PHYSICS*, **12** (4), pp. 264–274.

Kornowski, G., Yehudai, G., and Shamir, O. (2024). From tempered to benign overfitting in relu neural networks. *Advances in Neural Information Processing Systems*, **36**.

Kou, Y., Chen, Z., Chen, Y., and Gu, Q. (2023). Benign overfitting in two-layer relu convolutional neural networks. In *International Conference on Machine Learning*, PMLR, pp. 17615–17659.

Le Viet, H., Ngoc, H. L. H., Minh, K. T. D., and Van Hong, S. T. (2024). A deep learning framework for gym-gesture recognition using the combination of transformer and 3d pose estimation. *CYBERNETICS AND PHYSICS*, **13** (2), pp. 161–167.

Li, G., Gao, S., Luo, S., Zhou, L., Zhang, X., Cui, F., Zhao, H., and Feng, X. (2024). Tailoring macrostructure and texture in bobbin-tool friction stir weld via manipulation of deformation behaviour of plasticised metal during welding enabled by modifying tool profile. *International Journal of Machine Tools and Manufacture*, **201**, pp. 104198.

Li, J., Wu, X., Cao, L., Liao, B., Wang, Y., and Liu, Q. (2021). Hot deformation and dynamic recrystallization in al-mg-si alloy. *Materials Characterization*, **173**, pp. 110976.

Li, X., Lu, L., Li, J., Zhang, X., and Gao, H. (2020). Mechanical properties and deformation mechanisms of gradient nanostructured metals and alloys. *Nature Reviews Materials*, **5** (9), pp. 706–723.

Liu, W., Liu, Y., Cheng, Y., Chen, L., Yu, L., Yi, X., and Duan, H. (2020). Unified model for size-dependent to size-independent transition in yield strength of crystalline metallic materials. *Physical Review Letters*, **124** (23), pp. 235501.

Liu, X., Tian, S., Tao, F., and Yu, W. (2021). A review of artificial neural networks in the constitutive modeling of composite materials. *Composites Part B: Engineering*, **224**, pp. 109152.

Masi, F., Stefanou, I., Vannucci, P., and Maffi-Berthier, V. (2021). Thermodynamics-based artificial neural networks for constitutive modeling. *Journal of the Mechanics and Physics of Solids*, **147**, pp. 104277.

Masri, R. (2023). Exact formula for the effective yield stress of metals with arbitrary stress–strain curves. *International Journal of Impact Engineering*, **177**, pp. 104589.

Meng, Z., Qian, Q., Xu, M., Yu, B., Yıldız, A. R., and Mirjalili, S. (2023). Pinn-form: a new physics-informed neural network for reliability analysis with partial differential equation. *Computer Methods in Applied Mechanics and Engineering*, **414**, pp. 116172.

Minh, D., Wang, H. X., Li, Y. F., and Nguyen, T. N. (2022). Explainable artificial intelligence: a comprehensive review. *Artificial Intelligence Review*, pp. 1–66.

Nemat-Nasser, S. and Guo, W.-G. (2005). Thermomechanical response of hsla-65 steel plates: experiments and modeling. *Mechanics of Materials*, **37** (2-3), pp. 379–405.

Ng, C. W. W., Zhou, C., and Chiu, C. F. (2020). Constitutive modelling of state-dependent behaviour of unsaturated soils: an overview. *Acta Geotechnica*,

15 (10), pp. 2705–2725.

Pogorelko, V., Mayer, A., Fomin, E., and Fedorov, E. (2024). Examination of machine learning method for identification of material model parameters. *International Journal of Mechanical Sciences*, **265**, pp. 108912.

Saeed, W. and Omlin, C. (2023). Explainable ai (xai): A systematic meta-survey of current challenges and future opportunities. *Knowledge-Based Systems*, **263**, pp. 110273.

Safina, L. R., Krylova, K. A., and Baimova, J. A. (2022). Molecular dynamics study of the mechanical properties and deformation behavior of graphene/metal composites. *Materials Today Physics*, **28**, pp. 100851.

Savaedi, Z., Motallebi, R., and Mirzadeh, H. (2022). A review of hot deformation behavior and constitutive models to predict flow stress of high-entropy alloys. *Journal of Alloys and Compounds*, **903**, pp. 163964.

Shen, F., Münstermann, S., and Lian, J. (2020). An evolving plasticity model considering anisotropy, thermal softening and dynamic strain aging. *International Journal of Plasticity*, **132**, pp. 102747.

Su, M., Yu, Y., Chen, T., Guo, N., and Yang, Z. (2024). A thermodynamics-informed neural network for elastoplastic constitutive modeling of granular materials. *Computer Methods in Applied Mechanics and Engineering*, **430**, pp. 117246.

Tiamiyu, A. A., Pang, E. L., Chen, X., LeBeau, J. M., Nelson, K. A., and Schuh, C. A. (2022). Nanotwinning-assisted dynamic recrystallization at high strains and strain rates. *Nature materials*, **21** (7), pp. 786–794.

Tricarico, M., Besnard, C., Cinque, G., Korsunsky, A. M., and Tan, J.-C. (2023). Stress–strain relationships and yielding of metal-organic framework monoliths. *Communications Materials*, **4** (1), pp. 86.

Veasna, K., Feng, Z., Zhang, Q., and Knezevic, M. (2023). Machine learning-based multi-objective optimization for efficient identification of crystal plasticity model parameters. *Computer Methods in Applied Mechanics and Engineering*, **403**, pp. 115740.

Wang, J., Li, T., Cui, F., Hui, C.-Y., Yeo, J., and Zehnder, A. T. (2021). Metamodeling of constitutive model using gaussian process machine learning. *Journal of the Mechanics and Physics of Solids*, **154**, pp. 104532.

Wang, J., Zhu, B., Hui, C.-Y., and Zehnder, A. T. (2023). Determination of material parameters in constitutive models using adaptive neural network machine learning. *Journal of the Mechanics and Physics of Solids*, **177**, pp. 105324.

Xu, K., Huang, D. Z., and Darve, E. (2021). Learning constitutive relations using symmetric positive definite neural networks. *Journal of Computational Physics*, **428**, pp. 110072.

Xu, X. and Gu, Y. (2023). Benign overfitting of non-smooth neural networks beyond lazy training. In *International Conference on Artificial Intelligence and Statistics*, PMLR, pp. 11094–11117.

Xu, Z. and Huang, F. (2013). Thermomechanical behavior and constitutive modeling of tungsten-based composite over wide temperature and strain rate ranges. *International Journal of Plasticity*, **40**, pp. 163–184.

Yegnanarayana, B. (2009). *Artificial neural networks*. PHI Learning Pvt. Ltd.

Yuan, L., Ni, Y.-Q., Deng, X.-Y., and Hao, S. (2022). A-pinn: Auxiliary physics informed neural networks for forward and inverse problems of nonlinear integro-differential equations. *Journal of Computational Physics*, **462**, pp. 111260.

Zerilli, F. J. and Armstrong, R. W. (1987). Dislocation-mechanics-based constitutive relations for material dynamics calculations. *Journal of applied physics*, **61** (5), pp. 1816–1825.

Zerilli, F. J. and Armstrong, R. W. (1996). Constitutive relations for titanium and ti-6al-4v. In *Proceedings of the conference of the American Physical Society topical group on shock compression of condensed matter*, vol. 370, pp. 315–318.

Zhang, D., Zhang, X.-M., Nie, G.-C., Yang, Z.-Y., and Ding, H. (2021a). Characterization of material strain and thermal softening effects in the cutting process. *International Journal of Machine Tools and Manufacture*, **160**, pp. 103672.

Zhang, H., Xiao, H., Fang, X., Zhang, Q., Logé, R., and Huang, K. (2020). A critical assessment of experimental investigation of dynamic recrystallization of metallic materials. *Materials & Design*, **193**, pp. 108873.

Zhang, J., Yi, Y., Huang, S., Mao, X., He, H., Tang, J., Guo, W., and Dong, F. (2021b). Dynamic recrystallization mechanisms of 2195 aluminum alloy during medium/high temperature compression deformation. *Materials Science and Engineering: A*, **804**, pp. 140650.

Zhang, X., Zhu, Y., Wang, J., Ju, L., Qian, Y., Ye, M., and Yang, J. (2022). Gw-pinn: A deep learning algorithm for solving groundwater flow equations. *Advances in Water Resources*, **165**, pp. 104243.

Zhao, S., Petrov, Y. V., Zhang, Y., Volkov, G., Xu, Z., and Huang, F. (2024). Modeling of the thermal softening of metals under impact loads and their temperature–time correspondence. *International Journal of Engineering Science*, **194**, pp. 103969.

Zhu, Y., Gong, Q., and Yi, M. (2024). Molecular dynamics investigation of shock-induced deformation behavior and failure mechanism in metallic materials. *Archives of Computational Methods in Engineering*, **31** (4), pp. 2317–2344.

Zou, J., Han, Y., and So, S.-S. (2009). Overview of artificial neural networks. *Artificial neural networks: methods and applications*, pp. 14–22.